Halo polarization profiles and the interfacial angles of ice crystals

G. P. Können, Sara H. Muller, and J. Tinbergen

Polarization and radiance of various types of refraction halo in ice-crystal swarms that extend to ground level were measured as a function of scattering angle. Simultaneously, samples of the crystals that produce these halos were collected and replicated. The halo polarization peaks are wider than the Fraunhofer theory of diffraction predicts for the observed size distribution of the replicated crystals. The explanation we put forward is that the angles between crystal prism faces are not always exact integer multiples of 60°, and the basal faces are not always exactly parallel, as is usually assumed. The collected crystals confirm this. The widths of the halo polarization peaks can be explained if the distributions of the interfacial angles around their means reach their half-maximum values at a deviation of 0.49° ± 0.05°. This corresponds to a deviation of 0.35° ± 0.03° of the face normals from their crystallographic positions. The presence of variation in interfacial angles in low-level halos seems to arise from the fact that the crystals are growing. Some hitherto unexplained features in halo displays can be understood by considering variations in the interfacial angles.

Key words: Halos, polarization, ice crystals, atmospheric optics.

1. Introduction

During Antarctic halo displays arising from low-level crystal swarms, the radiance (often loosely called intensity) and the degree and direction of linear polarization were recorded as a function of scattering angle, for various types of halo. Simultaneously, three-dimensional replicas of falling ice crystals were made at ground level in acrylic spray. The main purpose of this was to provide an experimental check of the theories that have been used to relate the width of the halo polarization profile[1] or the excess broadening of the radiance profile[1–3] to the sizes of the halo-generating ice crystals. The field work for this investigation was carried out by one of us[4] at the U.S. South Pole station during the austral summer of 1989–1990, with an extention at the Russian station Vostok, during the following summer. The results and analysis are presented in this paper.

J. Tinbergen is with the Kapteyn Observatory, Mensingheweg 20, 9301 KA Roden, The Netherlands; the other authors are with the Royal Netherlands Meteorological Institute, P.O. Box 201, 3730 AE De Bilt, The Netherlands.

Received 17 November 1993; revised manuscript received 18 February 1994.

0003-6935/94/214569-11$06.00/0.

2. Theory

For the interpretation of the observational results we apply the theory of halo polarization as presented previously.[1] Its approach is as follows. First, it calculates the relation between the angular radiance of a refraction halo and its polarization as caused by Fresnel losses at refraction and by birefringence of the crystals. Then a formula for the halo angular radiance, which is valid for geometric optics, is substituted. This yields a formula for the halo polarization profile in terms of Stokes parameters. The angular distribution in the formulas for the radiance and the Stokes parameters are sharper than observed. There are several reasons for this: departures from geometric optics, the width of the solar disk, and so on. The broadening mechanisms are then described separately by a broadening function g, which is subsequently convolved with the idealized functions for radiance and Stokes parameters to transform them into more realistic functions.

In the paper we use the (I, Q, U, V) notation for the Stokes parameters; these are all in units of radiance, i.e., flux per unit of solid angle in the sky and per unit area of a detector. V, which describes circular polarization, need not be considered, as circular polarization is absent in ice-crystal halos. In Subsection 2.A the formulas for halo polarization are outlined, and in Subsection 2.B the properties of the halo-broadening

function are discussed for Fraunhofer diffraction and a realistic size distribution of the crystals.

A. Halo Polarization

The effect of birefringence of ice crystals on the polarization of refraction halos is depicted schematically in Figs. 1 and 2. Birefringence results in a polarization dependence of the index of refraction. This causes a refraction halo to consist of two components with different polarization states and shifted slightly in angle with respect to each other. As a consequence, the halo polarization profile may differ considerably from its radiance profile.

We consider the halo radiance I and the second and third Stokes parameters (Q, U). A proper choice of the plane of reference of the Stokes parameters ensures that $U = 0$. This is often achieved when the scattering plane is taken as reference; for parhelia the horizontal plane is the logical choice. By doing so, the state of linearly polarized light can be described by (I, Q), where Q represents the intensity transmitted through an ideal polarizer with its transmission axis parallel to the Stokes parameter reference plane minus the intensity that is transmitted after a 90° rotation of the polarizer; Q/I is the degree of linear polarization.

Let θ be the scattering angle and let $[I_g(\theta), Q_g(\theta)]$ be the halo radiance and the second Stokes parameter calculated according to geometric optics, where the source of illumination is a point source located at infinity; $[I_H(\theta), Q_H(\theta)]$ refers to the situation in which the halo is broadened. The broadening is described by the convolution of $[I_g(\theta), Q_g(\theta)]$ and a normalized function $g(\theta)$:

$$[I_H(\theta), Q_H(\theta)] = \int_{-\infty}^{\infty} [I_g(x), Q_g(x)]g(x - \theta)dx. \quad (1)$$

The broadening function $g(\theta)$, yet to be specified, may account for the various independently acting broadening mechanisms, like solar-disk smearing and smearing that is due to the wavelength dependence of the halo angle θ_h, as well as for smearing that is due to diffraction.

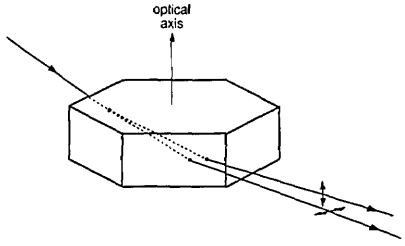

Fig. 1. As a result of birefringence, a light ray entering an ice crystal is split into two polarized rays with slightly different paths through the crystal. The direction of polarization of the ordinary refracted ray is perpendicular to the plane formed by the ray and the optical axis; that of the extraordinary ray is parallel to such a plane. For ice, the ordinary refracted ray is the least refracted. Each polarization forms its own halo.

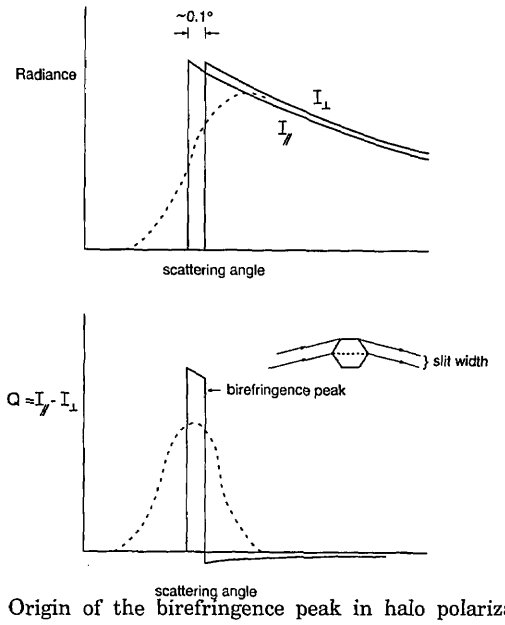

Fig. 2. Origin of the birefringence peak in halo polarization. Because of birefringence, the halo consists of two orthogonally polarized components (Fig. 1). For 22° halos, the component with polarization in the plane of scattering is closest to the Sun. Its radiance is denoted by $I_\parallel$, that of the other component is denoted by $I_\perp$. $I_\parallel - I_\perp$ equals the first Stokes parameter Q if the plane of reference of the Stokes parameters is the scattering plane. The solid curves give the situation for geometric optics; the dashed curves include broadening, e.g., by diffraction. Because in geometric optics the peak in Q is so narrow, the shape of the broadened Q peak closely resembles that of the broadening function. If diffraction were the main cause of the broadening, the width of this broadened peak would be determined by the slit width of rays emerging from the crystal and hence by the crystal diameter. Differences in $I_\perp$ and $I_\parallel$ that are due to Fresnel losses at refraction are not depicted in this schematic figure.

The difference in halo angle between the two polarized halo components is denoted by $\Delta\theta_h$, which is positive when the smaller of the two halo angles is that of the component with polarization parallel to the reference plane of the Stokes parameters. For the 22° circular halo and related types of halo like the parhelion, its value is +0.11°; for the 46° circular halo and related types it is −0.15°. The ratio F of the radiances of the polarized components with polarization perpendicular and parallel to the reference plane is determined by the Fresnel coefficients of refraction. We define

$$P_{\text{Fresnel}} = \frac{1 - F}{1 + F}. \quad (2)$$

This quantity is the degree of polarization that would occur in the absence of birefringence for halos arising from refraction in the normal plane, which is a plane prependicular to the edge formed by the faces where the light enters and leaves the crystal. For halos with a skew ray path through the crystal, such as the parhelion, P_{Fresnel} is somewhat less than the polarization that would arise from the same path through an isotropic crystal. P_{Fresnel} is positive; its

weak dependence on θ is neglected in the calculation below.

The relation between $Q_g(\theta)$ and $I_g(\theta)$ for halos generated by weakly birefringent crystals is given by Eq. (7) of Ref. 1. After substitution of Eq. (2) it reads

$$Q_g(\theta) = 1/2[1 + P_{\text{Fresnel}}\text{sgn}(\Delta\theta_h)] \times \Delta\theta_h I_g(\theta_h)\delta(\theta - \theta_h) + P_{\text{Fresnel}} I_g(\theta) + 1/2\Delta\theta_h \frac{dI_g(\theta)}{d\theta}. \quad (3)$$

The first term of Eq. (3) is by definition the birefringence peak. Its width in scattering angle is represented by a δ function. This applies because $|\Delta\theta_h|$ is much smaller than the typical width of the broadening function $g(\theta)$. The convolution [Eq. (1)] of $g(\theta)$ and the first term of Eq. (3) is denoted by $Q_{\text{birefr}}(\theta)$ and represents the birefringence peak of the broadened halo.

For the convolution of the remaining two terms of Eq. (3), the angular distribution of scattered light according to geometric optics $I_g(\theta)$ is approximated[1] by an exponential function:

$$\begin{aligned} I_g(\theta) &= 0, && \theta < \theta_h \\ I_g(\theta) &\cong I_g(\theta_h)\exp[-\alpha(\theta - \theta_h)], && \theta \geq \theta_h, \end{aligned} \quad (4)$$

so that $dI_g(\theta)/d\theta = -\alpha I_g(\theta)$. Hence Eqs. (1) and (3) give two expressions for $Q_{\text{birefr}}(\theta)$:

$$Q_{\text{birefr}}(\theta) \propto g(\theta - \theta_h), \quad (5a)$$

$$Q_{\text{birefr}}(\theta) = Q_H(\theta) - (P_{\text{Fresnel}} - 1/2\alpha\Delta\theta_h)I_H(\theta). \quad (5b)$$

Equation (5b) permits the calculation of $Q_{\text{birefr}}(\theta)$ from the observed halo second Stokes parameter $Q_H(\theta)$, the observed radiance $I_H(\theta)$, and the calculated value of P_{Fresnel}; the required value of α follows from the decreasing part of $I_H(\theta)$. Expression (5a) relates $Q_{\text{birefr}}(\theta)$ directly with the broadening function $g(\theta)$.

B. Broadening Function $g(\theta)$ for Diffraction

Here we calculate halo broadening according to Fraunhofer theory for a cloud of crystals with a gamma-distributed diameter d of the hexagonal faces. We consider parhelia and the 22° halo. In the region of the halo angle the scattering crystals are near the minimum-deviation configuration. A crystal is assumed to act as a rectangular slit. The broadening in the θ coordinate is determined by the slit width a, which is the width of the outgoing light beam projected onto the scattering plane. Hence the slit width a is proportional to the hexagon diameter d; the slit length is proportional to the length l of the crystal, which is the distance between the basal faces. When the hexagon diameter d is specified here to be the distance between the first and the fourth vertices, $a/d = 0.38$ for a regular hexagon; for a hexagon with a shape between a regular triangle and a regular hexagon, a/d becomes larger but will never exceed 0.8. As the profile of Q_{birefr} is in general narrow, the values of a/d presented here apply to the entire profile of Q_{birefr}.

The relation between the mean length $\bar{l}$ of crystals with diameter d and d is often represented by a power law,[5] $\bar{l} \propto d^p$. For plates, realistic values of p can generally be bracketed between 0.5 and 1. We put $p = 1$ (aspect ratio $\bar{l}/d$ = constant) and estimate an absolute upper limit to the diffraction broadening by considering the extreme case $p = 0$ (l = constant).

The required broadening function $g(\theta)$ can be found from the integral of the differential scattering cross section for finite cylinders[6] over a gamma distribution[7] $N(a)$ of slit widths. If the distribution of $l(d)/\bar{l}(d)$ is independent of d, an additional integration over l is not required. Omitting the mean sign over the symbol l and approximating sin θ by θ, one has

$$g(\theta) \propto \int_0^\infty l^2 d^2 \frac{\sin^2 x}{x^2} N(a)da,$$

$$N(a) \propto a^n \exp(-\beta a),$$

$$x = \frac{\pi a}{\lambda}\theta, \quad a = 0.38d, \quad l \propto d^p, \quad \beta = (n + 1)/\bar{a}, \quad (6)$$

where n is the power of the gamma distribution, $\bar{a}$ is the mean slit width, and λ is the wavelength. If one puts $g(0) = 1$, expressions (6) lead to

$$g(\theta) = \frac{1}{y^2}[2 - (1 - iy)^{-m} - (1 + iy)^{-m}]/[m(m + 1)],$$

$$m = n + 2p + 1, \quad y = \frac{2\pi}{\beta\lambda}\theta, \quad i = \sqrt{-1}, \quad (7)$$

which for any m is a real function, and for $m \leq 14.4$ is a function without oscillations. The angular width $\theta_{1/2}$ from the maximum ($\theta = 0$) of $g(\theta)$ to its half-maximum points $1/2\ g(0)$ can be calculated with an accuracy within 1% from

$$y_{1/2} = \frac{11}{4m + 7}. \quad (8)$$

Putting $\lambda = 590$ nm and expressing $\bar{a}$ in micrometers gives, for a power-one gamma distribution ($n = 1$),

$$\theta_{1/2} = 0.18°\left(\frac{30}{\bar{a}}\right)\frac{22}{8p + 15}. \quad (9)$$

A Gaussian convolution rule may be used to calculate the total $\theta_{1/2}$ resulting from different processes:

$$\theta_{1/2}^2\,(\text{total}) = \theta_{1/2}^2\,(\text{diffraction}) + \theta_{1/2}^2\,(\text{solar smearing}) + \cdots. \quad (10)$$

Three final remarks have to be made. First, in the case of the parhelion, $\theta_{1/2}$ refers to the width in the horizontal rather than in the scattering angle, but for

the solar height of our observations this difference can be neglected. Second, geometric obstruction of skew rays by the basal faces and internal reflections at these faces may modify the shape of the emerging beam, hence affecting the relation between a and d for parhelia. In practice, however, the introduction of 10% uncertainty in this relation is sufficient to account for this. Third, expressions (6) and Eqs. (7)–(9) can also be applied to the 46° types of halo and to the vertical diffraction broadening of parhelia, if d and l are properly interchanged. Table 1 summarizes the procedure for this.

3. Observations

The observations described here were made at the U.S. Amundsen–Scott South Pole Station (90 °S) as part of an Antarctic halo project. Our purpose was to explore experimentally the link between the optical properties of halos and the sizes and shapes of halo-generating crystals. This requires measurements of various kinds during a halo display. We aimed for an observation set consisting of slide photographs, measurements of the angular distribution of radiance and polarization for various halos, replication of falling crystals, and a visual check of the visibility of the halos in front of a nearby black object. For this, a bright and well-defined halo display was needed, one that would persist for at least 20 min under stable conditions. This is rare even in Antarctica, but on two occasions the entire observational sequence was successfully completed.

A. Method

The polarization and radiance measurements of halos were obtained by means of the portable, calibrated four-lens monochromatic polarimetric camera[1] shown in Fig. 3. This camera, a rebuilt commercial camera for passport photographs, has a focal length of 125 mm and takes four photographs simultaneously on a single Kodak Tri-X sheet film negative. Behind each lens is a polarizer, cut from the same sheet and with its orientation increasing in steps of 45°; one of the polarizers has its transmission axis parallel with the horizontal axis of the camera. The light then passes through a glass color filter. Filter and emulsion responses define a passband of 33-nm full-width at half-maximum centered on 590 nm. The negatives were digitized with the Astroscan semispecular densitometer of the Observatory of Leiden University. After the photographic densities were converted to light exposures (quantities of light that came in per unit area of the negative) with a power law,[8] the light exposures in the pixels of the four images corresponding to the same area in the sky were compared. The sum of light exposures of corresponding pixels in two orthogonally polarized images provides the radiance I; its difference in one pair of orthogonally polarized images provides the second Stokes parameter Q in the frame of reference of the camera; the difference in the other pair defines the third Stokes parameter U. The camera has a spirit level and a Sun finder; if the Sun is centered in that finder, the camera points at 22° from the Sun, and the scattering angle in the images is known to within an accuracy of ~0.2°. Parhelion pictures were taken with the camera kept horizontal, circumzenithal arc pictures with the camera vertical.

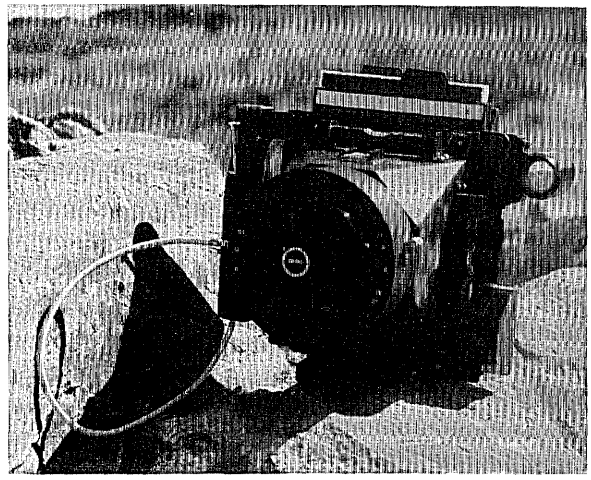

Fig. 3. Simple four-lens polarimetric camera that was used to record the angular distribution of polarization and radiance of halos.

The crystal replicas were made in acrylic spray. The procedure was as follows. A glass sheet covered by a thin layer of liquid acrylic spray was swept at a horizontal speed of ~1 m/s through the falling crystals surrounding us, some of which adhered to and submerged in the spray. After 5–10 s the acrylic spray layer had hardened enough to prevent any new penetration of crystals. The spray-covered glass was then kept for 6 h outside in the shade (temperature −25 °C) to permit sublimation of the crystals, leaving their imprints in the form of holes. After a successful sampling, the spray on the 5 cm × 5 cm glass sheet typically contained 30,000 crystals. The horizontal sweeping implies that the crystal number density in the air was measured; a check of the visibility of the halos in front of the nearby black object ensured that the replicated crystals were among those producing

Table 1. Parameters for the Calculation of Fraunhofer Diffraction Broadening[a]

Object	Slit Width a	Slit Length
22° circular halo, tangent arc, etc.	$0.38d$ (hexagons)	$\propto l$
	$0.76d$ (triangles)	$\propto l$
Parhelion, horizontal cross section	$0.38d$ (hexagons)	$\propto l$
	$0.76d$ (triangles)	$\propto l$
Parhelion, vertical cross section[b]	$l \cos h$	$\propto d$
46° circular halo, circumzenithal arc, etc.		
Plates ($l/d < 0.9$)[b]	$0.38l$	$\propto d$
Columns ($l/d > 0.9$)[c]	$0.32d$	$\propto d$

[a]Hexagon diameter d is the distance between first and fourth vertices, crystal length l is the distance between basal faces, and h is solar elevation. Values are for minimum deviation.

[b]For these cases, p in Eqs. (7) and (9) has to be replaced by p^{-1}.

[c]In this case, $p = 1$ in Eqs. (7) and (9).

the halos.[9] Simple visual inspection of a halo could easily confirm this when perspective effects are apparent and dynamic moving streaks in the halo, caused by the passing of nearby wind-driven crystals, could be seen.

B. Results

The two high-quality observation sets were obtained on 29 December 1989, 23:10–23:30 local time (LT), and 2 January 1990, 1:40–2:30 LT. On both occasions there was a bright display dominated by halos that were due to plate-orientated crystals (vertically oriented crystal C axes),[10] hence with a prominent appearance of the parhelia, the circumzenithal arc, the parhelic circle, and the 120° parhelion (Plates 20–23). Apart from photographs, the first set consists of one crystal sampling, three polarimetric pictures of a parhelion, and three of the circumzenithal arc. In some of the parhelion pictures the 22° circular halo is also visible. The second set contains two samplings, four polarimetric pictures of a parhelion, and four of the circumzenithal arc. The quality of the latter set is slightly superior, as the samplings, bracket polarimetric pictures and vice versa. A substantial addition to this set are two direct photographs of some tens of actual crystals, provided by W. Tape. He collected these crystals in Petri dishes, which contained hexane, during 1:41–1:43 LT and 2:00–2:04 LT, and, immediately after each collection, he photographed the crystals under a microscope. The crystal collection took place in the shade of the wind; during the collection the dishes were standing on a box ~70 cm high. The results of the polarimetry and the crystal sampling of both sets are similar; in this paper we focus on the data of the second display.

Table 2 summarizes the observations of the 2 January data set. It also includes the parameter α [Eq. (4)] representing the logarithmic slope of the parhelion radiance or the circumzenithal arc radiance in its decreasing part. The fluctuations of this parameter in time can be attributed to fluctuations in plate orientation in the passing crystal swarm: a smaller mean departure of the orientation of the crystal C axes from the zenith results in a larger α. Among the parhelia, the third picture (2:03 a.m.) has the largest α in the observation set. A consequence of the α value of that observation is that the transformation from Q to Q_{birefr} requires only a slight correction [Eq. (5b)].

For the presentation of the photopolarimetric measurements we selected for both the parhelion and the circumzenithal arc the data of their 2:03 a.m. picture. Figures 4 and 5 show one of the four images of the 2:03 a.m. polarimetric parhelion picture and a picture of some of the crystals replicated at 2:08 a.m., respectively. Figure 6 shows the parhelion radiance I and second Stokes parameter Q as a function of scattering angle, obtained from two of the four images on the digitized 2:03 a.m. negative. The cut presented in Fig. 6 passes straight through the radiance maximum of the parhelion. The plane of reference of the Stokes parameters is the horizontal, which closely coincides with the scattering plane. In the third Stokes parameter (not shown), the halo is not apparent, so the positive signal in Q indicates that the halo polarization is essentially horizontal. Note that the peak in Q occurs at a scattering angle different from that of the halo radiance peak, a feature that occurs for any halo whose polarization arises from birefringence.

The other polarimetric parhelion observations of 2 January are similar to Fig. 6, apart from the fact that they show a small tail in Q toward larger scattering angles. This tail arises because the terms on the right-hand side of Eq. (5b) do not cancel out. If corrected for this, a peak of similar width and shape as in Fig. 6 remains. We note that the α values of all our nearby Antarctic parhelia are lower than that of the high-level midlatitude parhelion ($\alpha = 1.0$ deg^{-1}), which is discussed in Ref. 1.

Figure 7 shows the photopolarimetric results of the circumzenithal arc. Strong polarization is present in a wide angular range; the reason is that refraction is the dominating mechanism. The drop in polariza-

Table 2. Polarimetric Observations and Crystal Replication during the South Pole Halo of 2 January 1990 (LT[a])

Time (a.m.)	Object	α (deg^{-1})[b]
1:42	Direct crystal photographing (W. Tape)	—
1:43	Parhelion	0.7
1:45	Circumzenithal arc	0.7
1:48	Crystal replicating	—
1:51	Parhelion	0.7
1:51	Circumzenithal arc	0.7
2:02	Direct crystal photographing (W. Tape)	—
2:03	Parhelion	0.8
2:03	Circumzenithal arc	0.5
2:08	Crystal replicating	—
2:17	Parhelion	0.5
2:17	Circumzenithal arc	0.7

[a]South Pole LT = UT + 12. The solar elevation was 23.0°.
[b]α is the logarithmic slope of the halo angular radiance distribution in its decreasing part.

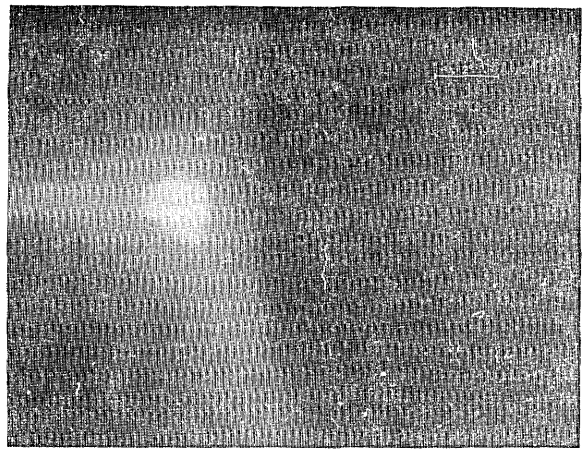

Fig. 4. South Pole parhelion and part of the 22° circular halo, photographed with the polarimetric camera on 2 January 1990, 2:03 a.m. Solar elevation was 23.0°; the Sun is to the right.

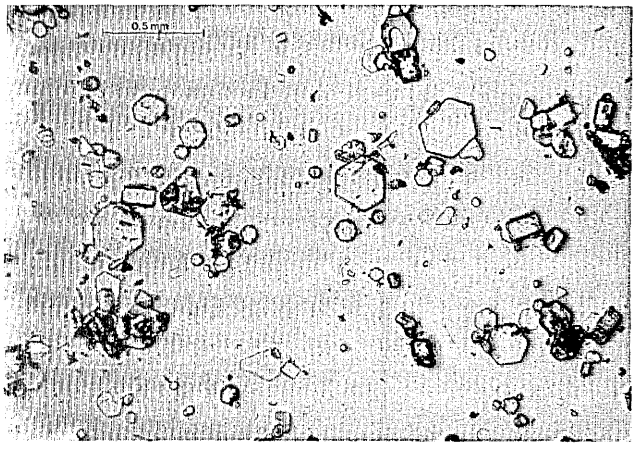

Fig. 5. Replicas of some crystals collected during the 2 January 1990 display at 2:08 a.m. Plates are visible as hexagons; columns have a rectangular envelope.

tion at lower scattering angles results from the birefringence peak, whose polarization for the 46° types of halo is perpendicular to the scattering plane. The Sun finder could not be used for the 46° scattering angle range, and hence the absolute value in the θ axis had to be guessed. In Fig. 7 it is assumed that the geometric halo angle for the circumzenithal arc coincides with the inflection point of the radiance, and an uncertainty of 2° in scattering angle is indicated.

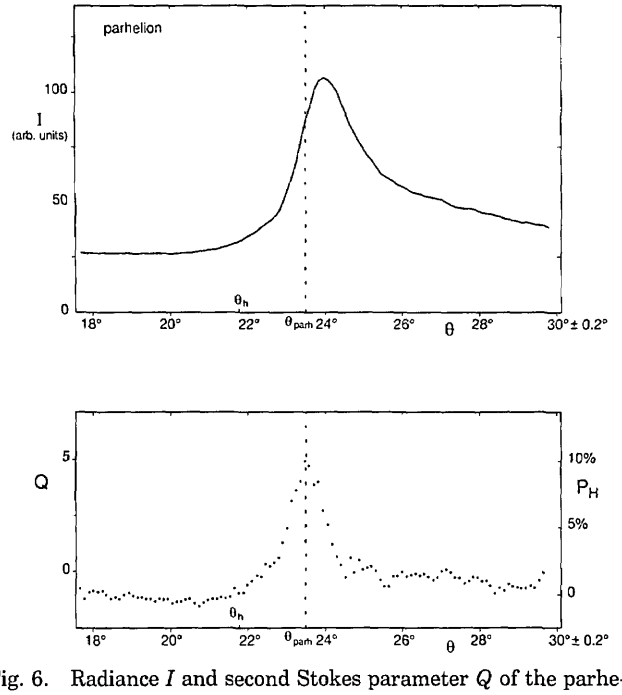

Fig. 6. Radiance I and second Stokes parameter Q of the parhelion of Fig. 4 as a function of scattering angle θ. The 22° halo angle (random crystal orientation) and the parhelion scattering angle (plate orientation) are denoted by θ_h and θ_{parh}, respectively. $Q > 0$ indicates horizontal polarization; Q/I is the degree of polarization of the total signal (halo plus background). P_H represents the scale for the intrinsic parhelion degree of polarization at θ_{parh}. The solar elevation was 23.0°.

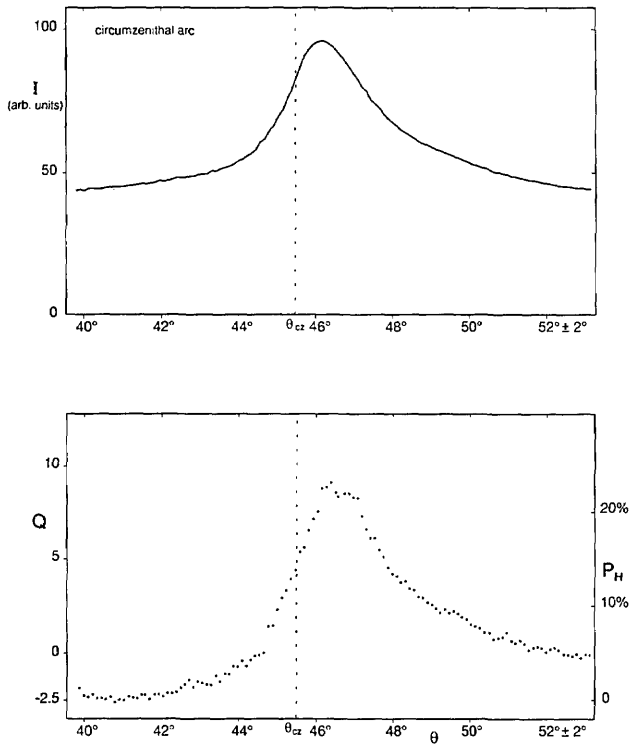

Fig. 7. Radiance I and second Stokes parameter Q of a circumzenithal arc. The display is the same as that of Fig. 6. The plane of reference of Q is the scattering plane, which coincides with the vertical and crosses the arc at a right angle; $Q > 0$ indicates vertical polarization. P_H represents the scale for the intrinsic degree of polarization of the arc at the scattering angle where Q is maximum. θ_{cz} is the halo angle for this arc. The solar elevation was 23.0°.

The observed values of α (Table 2) for circumzenithal arcs are low compared with what geometric optics predicts.[11,12] Apparently, for this type of halo, the angular width of the light distribution according to geometric optics is small compared with the broadening. This prevents a direct determination of α of the geometric-optical angular distribution of light [Eqs. (4)]. For the calculation of Q_{birefr} from Q [Eq. (5b)] an estimated value of $\alpha = 2$ was applied. Equation (5b) indicates that for circumzenithal arcs Q_{birefr} differs greatly from Q. We note, however, that the width of the peak in Q_{birefr} is not sensitive to the choice of α.

The crystals in the two replica samples (and that of 29 December 1989) are similar. Most crystals are thin plates lying flat on the spray-covered glass. The size distributions in the samples are almost indistinguishable. Figure 8 shows the hexagon size distribution of the crystals for the 2:08 a.m. sample, i.e., the number of cyrstals per unit size interval as a function of hexagon diameter, obtained by direct counting. The observed size distribution can be fitted with a gamma distribution with power one and a mean hexagon size $\bar{d}$ of 80 μm, the latter also being the observed value. The mean thickness of the plates was 30 μm. This number was inferred from the relatively rare cases in which a plate crystal left an imprint of its prism face. The relation between

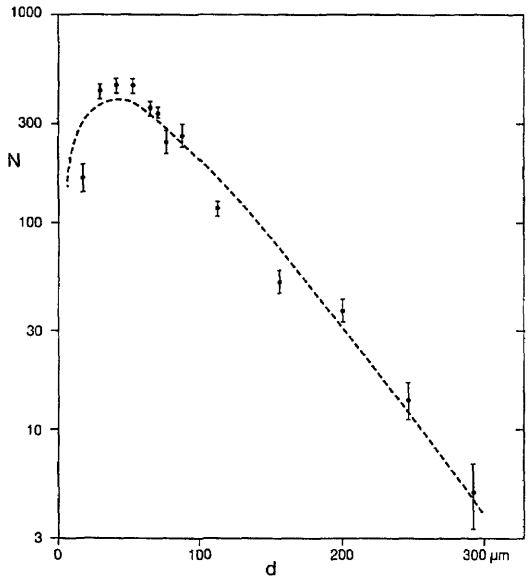

Fig. 8. Size distribution of the ice crystals collected during the halo display. The size d is the crystal hexagon diameter, specified here as the distance between the first and the fourth vertices, and N is the number of crystals per unit size interval. The error bars indicate the standard deviation in the determination of N. The dashed curve is a gamma distribution of power one for the observed mean size of 80 μm.

aspect ratio (crystal length divided by hexagon diameter) and hexagon size could not be determined quantitatively, although it seemed to decrease with size (see also Ref. 5). The replica sample also contained a small fraction of short columns. These may account for the appearance of the circular 22° halo (Fig. 4, Plates 20–23) and the faint upper tangent arc in Plates 20 and 21. The hexagon size distribution was found to be the same for the plates and the columns.

4. Discussion

A. Diffraction

Figures 9 and 10 show the birefringence peak Q_{birefr} for the parhelion and the circumzenithal arc, calculated with Eq. (5b) from the data. Also shown are the theoretical Q_{birefr} curves for diffraction, calculated from the observed gamma size distribution ($n = 1$) of the plate crystals in the replica sample; an aspect ratio constant [$p = 1$ in Eqs. (7)] is assumed here. The dashed curve in Fig. 9, which is for the extreme case, crystal length constant ($p = 0$), illustrates that the calculated Q_{birefr} profile is rather insensitive to the choice of p. Also, the width of the calculated curves depends little on the power of the fitting gamma distribution: even the extreme case in which Q_{birefr} is calculated from the poorly fitting power-two distribution ($n = 2$ with $\bar{d} = 80$ μm) widens the calculated width with respect to $n = 1$ by less than 30% [expressions (6) and Eqs. (7) and (8)]. In the calculation of the curves a size dependence[3] of the preference for plate orientation has not been taken into account; it can be shown that an inclusion of this dependence would narrow the curves by only a negligible amount,

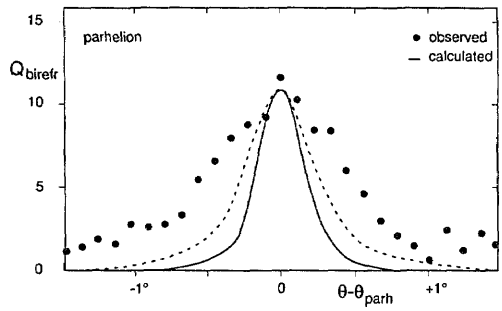

Fig. 9. Birefringence peak Q_{birefr} of the parhelion. $\theta - \theta_{\text{parh}}$ is the scattering angle minus halo angle for the parhelion. The filled circles are the observations as obtained from the measurements (Fig. 6) and Eq. (5b). The curves are Q_{birefr} for diffraction, calculated from the observed hexagon size distribution of the crystals by the use of Eqs. (7). The curves are scaled to match the observations at the maximum. The solid curve assumes a constant thickness-to-hexagon-diameter ratio (the more realistic assumption); the dashed curve assumes constant crystal thickness. All realistic cases are bracketed by these two extremes.

because of the rapid increase of the scattering cross section of crystals with size. It can also be shown that the values of Q_{birefr} of the observations (the filled circles in Figs. 9 and 10) are hardly sensitive to the power of the conversion law[8] used in the transformation from photographic density to radiance. In any case, there seems to be little agreement between the curves and the filled circles in Figs. 9 and 10; for the parhelion, the observed angular distance $\theta_{1/2}$ of 0.5° from maximum to half-maximum value is 2.5 times larger than the Fraunhofer diffraction by the sampled crystals predicts.

Our observations of the evolution of crystal-generating clouds led us to believe that the crystals in the good Antarctic displays were growing as they fell: often we saw a cumulus type of water cloud coming in, sometimes with a clear[13] fog bow in it, and then breaking up and turning to ice; subsequently, the halos appeared and we were surrounded by crystals, while in due course the sky turned from white to blue. Growing conditions mean that, averaged over the rising line of sight, the crystals are smaller than in

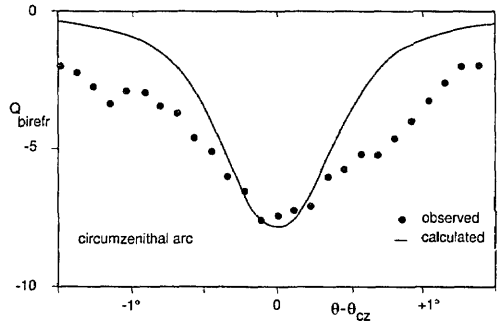

Fig. 10. Birefringence peak Q_{birefr} of the circumzenithal arc. $\theta - \theta_{\text{cz}}$ is the scattering angle minus the halo angle for the arc. The filled circles are the observations as obtained from the measurements (Fig. 7) and Eq. (5b). The curve is Q_{birefr} for diffraction, which is calculated from the observed crystal size distribution. A constant thickness-to-hexagon diameter [Eqs. (7)] is assumed.

the sample. When stationary conditions are assumed, the crystal size distribution in the line of sight and the resulting diffraction pattern can be calculated from the size distribution in the sample. This was done by means of a crystal growth-rate model[5,14] to calculate under the assumption of constant ice supersaturation for each sampled crystal the evolution of its size during the descent and by the use of the relation between size and terminal velocity[5] to transform the observed crystal number density in the air, as determned from the sample, into a vertical flux. The calculation implicitly assumes that the sampled crystals were among those producing the halos, which was proved by the observation that the halos remained visible in front of a nearby object.

However, the attempt to get a more reasonable fit with the observations by such a calculation failed completely. Even when the transformation from number density to flux was omitted, the new curves were only 10% wider than those in Figs. 9 and 10; with the transformation they are, in fact, 10% narrower than the original ones. The explanation for this failure is the dominant contribution by large crystals to the halo light, which is proportional to the scattering cross section and thus to the square of the linear crystal size. Hence the total amount of light that is scattered by a growing crystal during its lifetime is strongly determined by the very last part of its growing trajectory, where the crystal size is close to that at the moment of sampling.

Three other possibilities can be considered to solve the discrepancy between the observed width in Q_{birefr} and the calculation. The first one assumes the existence of a second population of crystals, higher up in the air. However, a simple calculation shows that a huge number of small crystals is required for producing the correct width of the diffraction curve. Also, the contribution of these hypothetical remote small particles to the halo radiance would completely dominate that of the nearby population. As this conflicts with the visual observations of the halos and with their intensity in front of the nearby black object, this explanation must be rejected. The second possibility is that the number of small crystals in the air is underestimated, as they are preferentially swept aside during the sweep in the process of sampling. However, Tape's pictures of crystals, which he collected in Petri dishes, do not show any evidence of the presence of many small crystals, let alone the huge number of them that is required for explaining the observed width in Q_{birefr}. The third possibility is a preferential contribution for $p \neq 1$ of small crystals to the parhelia radiance that is due to a size-dependent division of light between parhelion and subparhelion,[4] but this explanation is also not tenable. One reason is that a variance in aspect ratio causes this preference to disappear, but more importantly, the analysis of the 22° circular halo of Fig. 4 indicates the same width of Q_{birefr}, whereas for that halo a preference for smaller sizes should never occur.

The following conclusions can be drawn. First, the diffraction pattern calculated directly from the size distribution in the crystal sample is close to the diffraction pattern that will emerge from the crystal size distribution in the whole line of sight. Second, the observed width in the Q_{birefr} peak cannot be explained by Fraunhofer diffraction alone.

Table 3 summarizes the observations, the explained contribution is $\theta_{1/2}$, and the unexplained residue, calculated with Eq. (10). It also includes $\theta_{1/2}$ for the radiance in vertical direction of the parhelion, a parameter that we need below.

B. Crystal Alignment

The degree of imperfection of plate orientations can be quantified by $C_{1/2}$, which represents the mean departure of the orientation of the crystal C axes from the zenith. If crystals are not perfectly plate oriented, and hence $C_{1/2} \neq 0$, the resulting halos can be smeared out. This may in principle account for the unexplained part of Table 3, but is not strong enough. As to the observed circumzenithal arc, the width of the birefringence peak is in fact insensitive to variations in $C_{1/2}$. The reason is that the solar elevation differed very little (0.3°) from that at which the portion of the arc right over the Sun is formed by minimum deviation refraction. For the parhelion, imperfect orientation does widen the birefringence peak. However, a $\theta_{1/2} = 0.44°$ broadening by imperfect alignment would also cause $\theta_{1/2} = 1.3°$ for the broadening of the angular radiance distribution of the parhelion in the vertical. This is more than observed. Attributing the $\theta_{1/2} = 1.0°$ value in Table 3 for the vertical broadening completely to imperfect orientation leaves an unexplained value of $\theta_{1/2} = 0.27 \pm 0.03°$ in the broadening of the parhelion birefringence peak; the unexplained part of the circumzenithal arc broadening remains unchanged. Of course, the latter also holds for the circular 22° halo, which we mentioned above. Apparently an

Table 3. Distance $\theta_{1/2}$ in Scattering Angle from Maximum to the Half-Maximum Points (deg), 2 January 1990 Display

Object	Observed	Explained			Unexplained[c]
		Diffraction[a]	Solar Smearing	Wavelength[b]	
Circumzenithal arc, birefringence peak	0.80 ± 0.05°	0.39 ± 0.06°	0.12°	0.11°	0.68 ± 0.07°
Parhelion, vertical extent in radiance	1.00 ± 0.07°	0.16 ± 0.03°	0.12°	0	0.98 ± 0.07°
Parhelion, birefringence peak	0.50 ± 0.02°	0.19 ± 0.02°	0.12°	0.04°	0.44 ± 0.02°

[a]The uncertainty intervals extend from $p = 0.5$ to $p = 1$.
[b]Broadening is determined by the wavelength dependence of halo angle and the camera passband.
[c]Calculated with Eq. (10).

additional mechanism is required for explaining the width of the halos in our Antarctic data set.

C. Variations in the Interfacial Crystal Angles

Critical inspection of the shapes of the crystal replicas by one of us (S. Muller) revealed that the angles between the prism faces of ice crystals were not always exact integer multiples of 60°. It is directly apparent by the nonparallellism of opposite hexagon faces. This was first seen in some of the crystals of Fig. 5. In Fig. 11 the most prominent example that we could find in the replica is shown. In the right-hand marked crystal, the angle between one opposite pair of faces is 15°, and that between a second pair is 4°. In the other marked crystal, angles of ~2° are apparent. The phenomenon is real, as it persists when the (preserved) replicas are examined at different angles under the microscope. Melting cannot have been responsible for the formation of nonparallel planar faces, as melting leads to a complete deformation of the boundaries of a crystal replica. Another possibility is that the crystals broke in pieces when they hit the replicating spray. Although it is known that the preferential direction of fractures is parallel with a prism face or a basal face,[15] fractures in another direction cannot be excluded. However, it seems unlikely that breakings in unusual directions would occur along almost perfectly straight faults, and, apart from this, it is hard to believe that breaking alone would frequently produce crystals such as those in Fig. 11 with more than one pair of nonparallel faces. Interfacial angular variations were detected by us not only in replicated crystals, but also in some of the crystals photographed directly by W. Tape. The variation in angles may arise from the submicrometer stepped layers on the faces[13,16] of crystals that are growing; a temporal evaporation, for instance in the lower layers, may also result in strange angles. A growing ice crystal with a large variation in interfacial angles is shown in Plate I of Ref. 16.

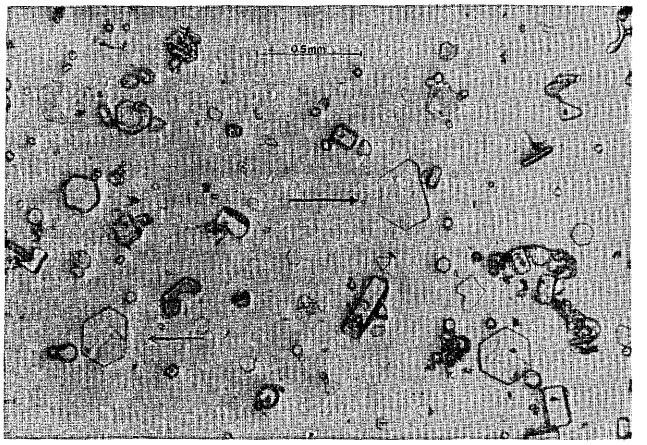

Fig. 11. Selected part of the 2:08 a.m. crystal replica sample that shows some crystals with a clear deviation from 120° in the angles between the prism faces. Note the nonparallellism of some pairs of opposite hexagon faces.

Table 4 summarizes for 23.0° solar elevation the effect of variations in crystal angles and of an imperfect alignment (see Subsection 4.B) of the ice crystals on the halo broadening. The variation in angle is represented by $A_{1/2}$, the nonideal crystal alignment by $C_{1/2}$. Again, the parameters refer to the distance in the distribution from the maximum to the half-power points. Also included in Table 4 are the values for these parameters that follow from the observed $\theta_{1/2}$, calculated with Eq. (10). The last column of Table 4 indicates that the observations can be explained if the distribution of interfacial angles has its half-maximum points at ~0.5° from its mean.

Within the experimental uncertainty the variation of the interfacial angles $A_{1/2}$ as derived from the parhelion and the circumzenithal arc is the same. Although encouraging at first sight, this result is not obvious. First, the ice crystals are nonspherical falling particles surrounded by an asymmetrical flow that may result in preferential growth at certain places at the crystal; second, ice is anisotropic. Despite these arguments no detectable anisotropy in $A_{1/2}$ is found. The mean of the two determinations in Table 4 yields $A_{1/2} = 0.49° \pm 0.05°$. This corresponds to a mean deviation $\delta_{1/2}$ of the actual face normals from their crystallographic positions of $A_{1/2}/\sqrt{2} = 0.35° \pm 0.03°$, which is the same for all faces.

The $C_{1/2}$ value in Table 4 is unexpectedly high; the width of the parhelic circle of Plate 22 rather suggests an upper limit of $C_{1/2}$ of 1°. However, the calculation of the vertical parhelion broadening ignored the contributions of rays that are subject to additional reflections at inclined basal faces. A parhelion from a ray path with two internal reflections and with $A_{1/2} = 0.5°$ for the basal faces has a vertical extent $\theta_{1/2}$ of 1°; four internal reflections lead to $\theta_{1/2} = 2°$. The relative contribution of the different ray paths to the parhelion is not known, but it is clear that any contribution of multiple-reflection ray paths will increase the vertical extent of the parhelion. This implies a smaller value of $C_{1/2}$ than the one presented in Table 4. Substitution of a low value of $C_{1/2}$ in the last line of Table 4 causes anisotropy in $\delta_{1/2}$ and raises the value of $A_{1/2}$ as derived from the parhelion birefringence peak to maximally 0.8°.

The variation $A_{1/2}$ found here is typical for our Antarctic observations. However, this result may not apply to other situations, as bright and well-defined Antarctic displays like the ones we could explore seem to occur under specific conditions. Visual inspection of the clouds during such displays as well as the unimodal size distribution in the crystal samples that we collected on these occasions suggest that in all cases the crystals originated from one level. Mostly, the mean crystal size on the different occasions was comparable, which indicates that the height of this level was similar.[13] Perhaps a further evolution of the growing crystals may result in another $A_{1/2}$.

It seems likely that varying crystal angles are a feature of crystals that are growing or perhaps evapo-

Table 4. Effect of Nonideal Crystal Alignment and Nonideal Interfacial Crystal Angle on Halo Broadening $\theta_{1/2}$ for Solar Elevation 23.0° and λ = 590 nm, 2 January 1990 Display

Object	$\theta_{1/2}$, Unexplained Value of Table 3 (deg)	Imperfect Orientation[a]	Imperfect Crystal Angles[a]	Results for $A_{1/2}$, $C_{1/2}$ (deg)
Circumzenithal arc, birefringence peak	0.68 ± 0.07	—	$\theta_{1/2} = 1.45\,A_{1/2}$ }	→ $A_{1/2} = 0.47 \pm 0.05$
Parhelion, vertical extent in radiance	0.98 ± 0.07	$\theta_{1/2} = 0.31\,C_{1/2}$	$\theta_{1/2} = 0.42\,A_{1/2}$	$A_{1/2} = 0.51 \pm 0.06$
				$C_{1/2} = 3.1 \pm 0.2$
Parhelion, birefringence peak	0.44 ± 0.02	$\theta_{1/2} = 0.11\,C_{1/2}$	$\theta_{1/2} = 0.55\,A_{1/2}$	

[a] $\theta_{1/2}$ is the width of the halo, $C_{1/2}$ is the departure of the orientation of the crystal C axes from the zenith, $A_{1/2}$ is the departure of the interfacial crystal angle from 90° (circumzenithal arc) or 60°(parhelion). $\theta_{1/2}$, $C_{1/2}$, and $A_{1/2}$ refer to the distance in the distributions from the maximum to the half-maximum points.

rating and hence are typical for low-level halo displays. Our midlatitude polarimetric observations of parhelia in high clouds seem to support this view. Neither in the parhelion discussed earlier[1] nor in two others scanned later (unpublished) does the width of the birefringence peak clearly exceed the width of the solar disk. This indicates large crystals with no detectable variation in their interfacial angles; it is reasonable to assume that the crystals causing these parhelia were in equilibrium with the vapor. The latter condition probably also applies to the crystals that caused the 22° circular halo at La Palma, which we scanned in multiwavelength polarimetry[1]; the wavelength dependence of the broadening of that halo (Fig. 14 of Ref. 1) is consistent with diffraction, and no excess broadening that is due to varying interfacial crystal angles is apparent. On the other hand, we cannot exclude that even a small growth rate may result in detectable interfacial variations. An indication for this came from a polarimetric observation (solar elevation 14.7°, no crystal sampling) of a parhelion in a low-level aircraft condensation trail at the Antarctic station Vostok on 7 January 1991. The trail had persisted for 3.5 h without showing any halo. Then the apparently slowly growing crystals produced a well-defined parhelion with an angular readiance distribution that looked quite similar to that of the midlatitude parhelia (like Fig. 16 of Ref. 1, and with $\alpha = 1.1\ \text{deg}^{-1}$) but with a $\theta_{1/2} = 0.5°$ broadening of its birefringence peak.

D. Observational Implications

Some rare halos in the Antarctic displays require an almost perfect orientation of the crystals. This is for instance the case with the Wegener arc and the subhelic arc.[10] A puzzling observation so far is the relatively diffuse appearance of accompanying halos, such as the upper tangent arc. The combination of an almost perfect alignment and variation in interfacial crystal angles does explain this paradoxical observation; the halo broadening would then be governed by the variations in the interfacial angles.

The consequences of interfacial variations in crystal angles on the frequency of halos that are due to multiple internal reflections, like the heliac arc,[10] are not clear. It should be explored with a Monte Carlo halo simulation program[17] for scattering by crystals with varying interfacial angles. The simulations may also represent the characteristic broadening of low-level halos (Plates 24 and 25) in a realistic way, even without the incorporation of diffraction.[18]

High-level midlatitude halos show a great variability in their appearance. This is often attributed to varying particle sizes, crystal-density fluctuations, or extinction. The occasional appearance of bright, well-defined but diffuse parhelia with a large vertical extent might be explained by interfacial angular variations that occur in crystals while they are growing. The shape and the light distributions of such parhelia may sometimes come close to that (Plate 4) of low-level display parhelia.

For the inverse problem, size determination from halo observations,[1–3,19] interfacial angular variations restrict the possibilities. As long as this factor is unknown, the width of the halo provides only a lower limit to the crystal size, unless a wavelength dependency of the width can be established. A problem that remains is to link an optically determined size to the real size when the size distribution is unknown. It is by no means obvious that high-level crystals have the same size distribution as the low-level ones; the distribution observed during the Antarctic displays may just represent an early stage, to be evolved to another distribution when the size grows. As long as this ambiguity remains, the optical broadening can provide only a characteristic size, such as the diameter that contributes most to the scattered intensity[4] or the so-called effective diameter, which is cross-sectional weighted size. An advantage of the latter parameter in this particular problem is that it depends little on the size distribution, as can be demonstrated from expressions (6) and Eq. (8) for gamma distributions of different powers.

As the variability in interfacial angles is probably a specific feature of crystals that are not in equilibrium, it is mainly significant for low-level halo displays. High-level displays are probably more frequently due to normally shaped crystals. In any case, high-level displays usually produce less interesting halos. The most complex displays are reported in low-level crystal clouds in cold climates, and they produce the halos that cry out for complete understanding. Interfacial angular variations seem a nonnegligible factor in this.

5. Conclusions

Evaluation of the radiance and the polarization profiles of Antarctic low-level halos and of the sizes and shapes of the crystals that were collected at ground level leads to the following conclusions:

- The diffraction broadening of low-level halos as calculated from the observed crystal sizes at ground level can be considered to be representative of the broadening that will result from all crystals in the line of sight.
- The halo broadening is too large to be explained by Fraunhofer diffraction and the observed crystal sizes.
- The angles between the prism faces of the ice crystals are not always exact integer multiples of 60°, and the basal faces are not always parallel. The halo broadening indicates an average deviation $\delta_{1/2}$ of $\sim 0.35°$ (distance between the maximum and the half-maximum points) of the normals of the crystal faces from their crystallographic positions. This corresponds to an average deviation in interfacial angles of 0.5°. A small difference between $\delta_{1/2}$ for prism and basal faces cannot be excluded.
- The observed variability in interfacial angles seems to be related to the special conditions in low-level swarms, in which the crystals are increasing in size as they fall. This variability restricts the possibilities for particle sizing by optical remote sensing.
- We recommend that variations of interfacial angles be included in Monte Carlo simulations of ice-crystal halo displays in order to explore the consequences of such variations for halo broadening and their possible significance in explaining rare halos.

The field work has been performed in cooperation with W. Tape; J. H. M. van Lieverloo, Kiwa, assisted with the size determinations; and R. S. Le Poole provided assistance in the use of the Leiden University Astroscan densitometer. The camera was rebuilt by H. Deen, Kapteyn Observatory, Roden. The helpful discussions with H. C. van de Hulst are gratefully acknowledged. Two anonymous referees provided constructive comments. M. H. Kaltofen is thanked for her excellent technical support in the preparation of this paper. This research was supported by National Science Foundation grant DPP-8816515 and partly by the Netherlands Organisation for Scientific Research.

References

1. G. P. Können and J. Tinbergen, "Polarimetry of a 22° halo," Appl. Opt. **30,** 3382–3400 (1991).
2. D. K. Lynch and P. Schwartz, "Intensity profile of the 22° halo," J. Opt. Soc. Am. A **2,** 585–589 (1985).
3. A. B. Fraser, "What size of ice crystals causes the halos?" J. Opt. Soc. Am. **69,** 1112–1118 (1979).
4. G. P. Können, "Photopolarimetry of halos and ice crystal sizing," Antarct. J. U.S. **27**(5), 1992 Review Issue, 293–296 (1992).
5. H. R. Pruppacher and J. D. Klett, *Microphysics of Clouds and Precipitation* (Nijhoff, Dordrecht, The Netherlands, 1978), Chap. 2, p. 40; Chap 13, p. 448; Chap 10, p. 340.
6. C. F. Bohren and D. F. Huffmann, *Absorption and Scattering of Light by Small Particles* (Interscience, New York, 1983), Chap. 8, p. 209.
7. H. C. van de Hulst, *Multiple Light Scattering* (Academic, New York, 1980), Vol. 2, Chap. 19, p. 665.
8. G. Brown, J. Burdsall, E. J. Hahn, A. G. Millikan, F. J. Parrish, C. N. Nelson, S. D. Robson, And M. L. Scott, *Scientific Imaging with Kodak Films and Plates* (Eastman Kodak Company, Rochester, N.Y., 1987).
9. W. Tape, "Some ice crystals that made halos," J. Opt. Soc. Am. **73,** 1641–1645 (1983).
10. W. Tape, *Atmospheric Halos,* Vol. 64 of Antarctic Research Series (American Geophysical Union, Washington, D.C., 1994).
11. W. Tape, "Analytic foundations of halo theory," J. Opt. Soc. Am. **70,** 1175–1992 (1980).
12. G. P. Können, "Polarization and intensity distributions of refraction halos," J. Opt. Soc. Am. **73,** 1629–1640 (1983).
13. G. P. Können, *Polarized Light in Nature* (Cambridge U. Press, Cambridge, 1985), Chap. 30, p. 58.
14. P. V. Hobbs, *Ice Physics* (Clarendon, Oxford, 1974), Chap. 9, p. 544.
15. L. W. Gold, "Formation of cracks in ice plates by thermal shock," Nature (London) **192,** 130–131 (1961).
16. J. Hallett, "Faceted snow crystals," J. Opt. Soc. Am. A **4,** 581–588 (1987).
17. F. Pattloch and E. Tränkle, "Monte Carlo simulation and analysis of halo phenomena," J. Opt. Soc. Am. A **1,** 520–526 (1984).
18. Y. Takano and S. Asano, "Fraunhofer diffraction by ice crystals suspended in the atmosphere," J. Meteorol. Soc. Jpn. **61,** 289–300 (1983).
19. G. P. Können, A. A. Schoenmaker, and J. Tinbergen, "A polarimetric search for ice crystals in the upper atmosphere of Venus," Icarus **102,** 62–75 (1993).